Correlation in Fermi liquids: Analytical results for the local-field correction in two and three dimensions

A. Gold and L. Calmels
Laboratoire de Physique des Solides, Université Paul Sabatier, 118 Route de Narbonne, 31062 Toulouse, France
(Received 2 February 1993)

The local-field correction for the two-dimensional and the three-dimensional electron gas is calculated within a sum-rule version of the self-consistent approach of Singwi, Tosi, Land, and Sjölander. Correlation effects are studied. Results for $0.001 < r_s < 100$ are given where r_s is the random-phase-approximation parameter. An analytical expression for the static structure factor, representing a generalized Feynman-Bijl spectrum, is used in the calculation. We derive analytical expressions for the density dependence of the local-field correction and we compare the results for the ground-state energy for the interacting electron gas with Monte Carlo computations. The pair-correlation function and the compressibility are studied. Exchange and correlation effects for quantum wells and heterostructures are calculated: numerical and analytical results are derived. In two dimensions and at low density a roton structure in the plasmon dispersion is found. We discuss an instability in layered structures of two-dimensional electron gases.

I. INTRODUCTION

The random-phase approximation (RPA) is a very good theory to describe dielectric properties of the interacting electron gas in the high-density limit ($r_s < 1$).[1] r_s is the RPA parameter. Plasmon and electron-hole excitations are described by the RPA, and for small wave numbers (large distances) the RPA is exact. The local-field correction (LFC) takes into account corrections to the RPA due to the effects of exchange and correlation.[2] The repulsion hole around an electron due to the exchange repulsion and the correlation effects is described by the local field. The LFC is important for large wave numbers (small distances) and for small particle densities. A self-consistent approach for the LFC and the static-structure factor (SSF) was formulated by Singwi, Tosi, Land, and Sjölander (STLS).[3] The approach was used to calculate the LFC for three-dimensional[3] and two-dimensional electron gases.[4] Large r_s values have not been studied within the complete STLS approach.[3,4] For a review of the STLS approach, see Ref. 5.

Many-body effects in the interacting electron gas have been studied during the last 40 years.[1,2] The ground-state energy is the sum of the kinetic (kin) energy, the exchange (ex) energy, and the correlation (c) energy. The first two terms can be calculated analytically as $\varepsilon_{\rm kin} \propto 1/r_s^2$ and $\varepsilon_{\rm ex} \propto -1/r_s$. The correlation energy is difficult to calculate. Monte Carlo computations[6] and density-functional-theory computations[7] are presently the most accurate calculations for the correlation energy, and results have been published for three[6,7] and two dimensions.[8]

A sum-rule version of the STLS approach was recently used to calculate the LFC for a charged Bose gas at zero temperature.[9] For a Bose gas the only excitations are the collective plasmon excitations, and the SSF can be calculated analytically. Therefore, the sum-rule approach became simple for the Bose gas. For the electron gas an exact analytical form for the SSF is not available from the literature.

In the following we present an analytical form for the SSF of interacting electrons. For small r_s this SSF reproduces the Hartree-Fock results for the pair-correlation function and the ground-state energy. The proposed SSF is a generalized form of the SSF in the mean spherical approximation.[8] The LFC is included in the new SSF. The generalized SSF describes the Coulomb-interaction effects quantitatively correctly for small electron densities ($1 < r_s < 20$), where the collective modes become the important modes. We use this analytical expression for the SSF in order to obtain numerical results for the LFC of three- and two-dimensional electron gases for $0.001 < r_s < 100$ within the sum-rule approach. We show first that this simplified STLS approach is in good agreement with the full STLS approach and with Monte Carlo calculations for the ground-state energy,[6] by studying the electron gas in three dimensions. In the second part of the paper we study the electron gas in two dimensions and compare with Monte Carlo calculations for the ground-state energy.[8] We study finite extension effects for quantum wells and heterostructures in order to present results for realistic structures as used in experiments.

The paper is organized as follows. The analytical expression for the static-structure factor is described in Sec. II. In Sec. III we present results for the local-field correction in three dimensions. The LFC in two dimensions is evaluated in Sec. IV. In Sec. V we present results for the two-dimensional electron gas with finite width. The plasmon dispersion is studied in Sec. VI. An instability in a layered two-dimensional electron gas is treated in Sec. VII, and correlation and exchange effects are discussed. In Sec. VIII we compare for $r_s < 1$ some analytical results for the correlation energy from the literature with our numerical results. A one-sum-rule approach is

 ©1993 The American Physical Society

discussed in Sec. IX. We discuss our results in Sec. X. A short discussion of experimental results appears in Sec. XI. We conclude in Sec. XII.

II. STATIC-STRUCTURE FACTOR

The wave-vector-dependent dynamical susceptibility $\chi(\mathbf{q},\omega)$ determines the static structure factor $S(\mathbf{q})$ via[1]

$$S(\mathbf{q})=\frac{1}{\pi N}\int_0^\infty d\omega\,\mathrm{Im}[\chi(\mathbf{q},\omega)]\ . \tag{1}$$

N is the electron density. For Planck's constant we use $h/2\pi=1$. The electron-hole excitation spectrum and the plasmon excitation spectrum are hidden in $\chi(\mathbf{q},\omega)$. For an interacting electron gas the ω integral in (1) cannot be performed analytically. In order to calculate the SSF, both excitations are important. The collective excitation spectrum (plasmon excitations) $\omega_p(\mathbf{q})$ for small wave vector $\mathbf{q}$ is expressed as

$$\omega_p^2(\mathbf{q})=Nq^2V(\mathbf{q})/m\ . \tag{2}$$

m is the effective electron mass and $V(\mathbf{q})$ is the Coulomb-interaction potential in Fourier space.

Within the mean spherical approximation (MSA) (Ref. 8) the SSF was given as[10]

$$S_{\mathrm{MSA}}(\mathbf{q})=1/[1/S_0(\mathbf{q})^2+4mNV(\mathbf{q})/q^2]^{1/2}\ . \tag{3}$$

$S_0(\mathbf{q})$ is the SSF of the free-electron gas and contains the electron-hole excitations. It was noted in Ref. 8 that for $r_s<1$ the MSA is a good approximation to the exact SSF calculated within the Monte Carlo approach, and that it becomes wrong for $r_s>1$.

From the interacting Bose gas[9,11] we know that the SSF contains the LFC $G(\mathbf{q})$. In the following we use an analytical form of the SSF and we suggest the following generalized approximation (GA) expression:

$$S_{\mathrm{GA}}(\mathbf{q})=\left[\frac{1}{1/S_0(\mathbf{q})^2+1/S_p(\mathbf{q})^2}\right]^{1/2}\ . \tag{4}$$

The term $S_0(\mathbf{q})$ in (4) represents the particle-hole spectrum, and the second term represents the plasmon excitations. The SSF $S_p(\mathbf{q})$ for plasmons is defined as

$$S_p(\mathbf{q})=\{q^2/4mNV(\mathbf{q})[1-G(\mathbf{q})]\}^{1/2}\ . \tag{5}$$

With $\varepsilon(\mathbf{q})=\mathbf{q}^2/2m$ the SSF can be written as *a generalized* Feynman-Bijl expression

$$S_{\mathrm{GA}}(\mathbf{q})=\frac{\varepsilon(\mathbf{q})}{\{\varepsilon(\mathbf{q})^2/S_0(\mathbf{q})^2+\omega_p^2(\mathbf{q})[1-G(\mathbf{q})]\}^{1/2}}\ . \tag{6}$$

It is easy to see that $S_{\mathrm{GA}}(\mathbf{q})=S_0(\mathbf{q})$ for $e^2=0$, and for $G(\mathbf{q})=0$ we obtain $S_{\mathrm{GA}}(\mathbf{q})=S_{\mathrm{MSA}}(\mathbf{q})$. For small wave numbers we find the correct behavior of the SSF $S_{\mathrm{GA}}(q\to0)\propto q^{(d+1)/2}$ for quantum liquids with long-range Coulomb interactions in d dimensions. For large wave vectors we find $S_0(q>2k_F)=S(q\to\infty)=1$.

We note that for $r_s\ll1$, $S_{\mathrm{GA}}(\mathbf{q})$ gives a LFC in agreement within the Hartree-Fock approximation (HFA): exchange effects dominate correlation effects, resulting in the Hubbard expression[12] for the LFC. For $r_s>1$ the plasmon excitations are as important as the electron-hole excitations: for the LFC, correlation effects are as important as exchange effects. This crossover from exchange to exchange/correlation is included in $S_{\mathrm{GA}}(q)$, as will be shown in the following. From a first view, however, it is not evident that this crossover is included: the exchange term in (3) is proportional to $1/S_0(q\to0)\propto k_F\propto N^{1/d}$, while the correlation term in (3) is proportional to $1/S_p(q\to0)\propto N^{1/2}$.

III. ELECTRON GAS IN THREE DIMENSIONS

A. Model and theory

We consider an interacting electron gas in three dimensions. The RPA parameter for three-dimensional systems is described as $r_s=[3/4\pi N_3a^{*3}]^{1/3}$. $a^*=\varepsilon_L/me^2$ is the effective Bohr radius defined with the effective electron mass m, the background dielectric constant ε_L, and the electron charge e. The electron density N_3 defines the Fermi wave number k_F via $N_3=k_F^3/3\pi^2$. In the following we measure wave numbers q in units of $q_0=12^{1/4}/(r_s^{3/4}a^*)$ as $x=q/q_0$. The Coulomb-interaction potential in Fourier space is $V(q)=4\pi e^2/\varepsilon_Lq^2$. The SSF of the free-electron gas is given by $S_0(q<2k_F)=3q/4k_F-q^3/16k_F^3$ and $S_0(q\geq2k_F)=1$.[1]

In the STLS approach[3] the LFC is given by a one-dimensional q integral over the SSF, which via (1) is determined by the LFC. The coupled equations for the self-consistent STLS approach must be solved numerically. One can show that $G(x\ll1)\propto x^2$, and that $G(x\gg1)$ is constant.

B. Results

We suggest the GA expression for the LFC in three dimensions to be[9]

$$G_{\mathrm{GA}}(x)=r_s^{3/4}\frac{0.846x^2}{2.188C_{13}(r_s)+x^2C_{23}(r_s)}\ . \tag{7}$$

The expression for $G_{\mathrm{GA}}(x)$ can be interpreted as a Hubbard-type expression[12] for the LFC, where the values for $x\ll1$ and $x\gg1$ are determined by the parameters $C_{13}(r_s)$ and $C_{23}(r_s)$, respectively. Using the analytical expression for the LFC, we find[9]

$$1/C_{13}(r_s)=1.180\,203\int_0^\infty dx\,[1-S_{\mathrm{GA}}(x)] \tag{8}$$

and

$$1/C_{23}(r_s)=1.618\,123\int_0^\infty dx\,x^2[1-S_{\mathrm{GA}}(x)]\ . \tag{9}$$

These equations have been derived before for the Bose gas in three dimensions.[9] However, the SSF of bosons is different from the SSF of electrons.

Equations (8) and (9) can be discussed within three different approximations. With $S_{\mathrm{GA}}(x)=S_0(x)$, one gets $C_{13,\mathrm{HF}}(r_s)$ and $C_{23,\mathrm{HF}}(r_s)$, which are the Hartree-Fock parameters, and explicitly we find

$$C_{13,\mathrm{HF}}(r_s)=1.0956r_s^{1/4} \tag{10a}$$

and

$$C_{23,\mathrm{HF}}(r_s)=1.6911 r_s^{3/4} . \tag{10b}$$

Within the HFA we find the Hubbard (H) result[3,12]

$$G_H(q)=\frac{1}{2}\frac{q^2}{4k_F^2/3+q^2} . \tag{11}$$

Using $S_{\mathrm{GA}}(x)=S_{\mathrm{MSA}}(x)$, we derive the coefficients in the lowest-order plasmon-pole approximation: $C_{12,0}(r_s)$ and $C_{22,0}(r_s)$. These coefficients represent the results for a RPA-like approximation.

Note that $S_{\mathrm{GA}}(x)$ in (8) and (9) contains $G_{\mathrm{GA}}(x)$, which depends on r_s. Equations (8) and (9) are much easier to solve than the full STLS equations. We calculated $C_{13}(r_s)$ and $C_{23}(r_s)$ with a personal computer (Macintosh-Si) for $0.000\,01<r_s<400$. Some results are given in Table I. We find that $C_{23}(r_s)$ increases strongly with increasing r_s, and the r_s dependence of $C_{13}(r_s)$ is weaker than that of $C_{23}(r_s)$. For $r_s<0.01$ our numerical results are very near to the results in the HFA (see Sec. VIII A). The numerical results can be described by the following expressions:

$$C_{13}(r_s)=0.918 r_s^{0.19} \quad \text{for } 0.1<r_s<1 , \tag{12a}$$

$$C_{13}(r_s)=0.916 r_s^{0.134} \quad \text{for } 1<r_s<10 , \tag{12b}$$

$$C_{13}(r_s)=0.921 r_s^{0.129} \quad \text{for } 10<r_s<50 , \tag{12c}$$

and

$$C_{23}(r_s)=1.108 r_s^{0.58} \quad \text{for } 0.1<r_s<1 , \tag{13a}$$

$$C_{23}(r_s)=1.076 r_s^{0.55} \quad \text{for } 1<r_s<6 , \tag{13b}$$

$$C_{23}(r_s)=0.782 r_s^{0.725} \quad \text{for } 6<r_s<50 . \tag{13c}$$

The accuracy of these analytical expressions is about 2%. Clearly, $C_{i3}(r_s\ll 1)\approx C_{i3,0}(r_s\ll 1)\approx C_{i3,\mathrm{HF}}(r_s)$. For large r_s we find $C_{i3,0}(r_s\gg 1)=1$, and the self-consistent equations give results similar to the results for bosons (B): $C_{i3,\mathrm{HF}}(r_s)>C_{i3}(r_s)\approx C_{i3,B}(r_s)$.[9]

The difference between $C_{i3,\mathrm{HF}}(r_s)$ and $C_{i3}(r_s)$ is the result of correlation effects in the interacting electron gas. These correlation effects are small, if compared with the kinetic energy, for $r_s\ll 1$, but they are large for $r_s>1$.

TABLE I. Parameters for the local-field correction for $d=3$: $C_{13,0}$, $C_{23,0}$, C_{13}, and C_{23} according to (8) and (9) for various values of r_s.

r_s	$C_{13,0}(r_s)$	$C_{23,0}(r_s)$	$C_{13}(r_s)$	$C_{23}(r_s)$
0.01	0.344	0.053	0.344	0.053
0.04	0.478	0.144	0.479	0.146
0.1	0.586	0.266	0.589	0.278
0.4	0.760	0.569	0.777	0.666
1	0.863	0.780	0.905	1.090
4	0.960	0.957	1.107	2.290
10	0.987	0.990	1.243	4.102
40	0.998	1.000	1.477	11.46
100	1.000	1.000	1.674	23.37

Due to the analytical form of the SSF these correlation effects can be traced back to the plasmon dynamics in the system. Exchange effects already exist in the noninteracting electron gas, and are described by $S_0(q)$.

C. Application

The SSF determines the pair-correlation function $g(r)$. For $r=0$ one gets[2]

$$g(0)=1-1.368 r_s^{3/4}\int_0^\infty dx\, x^2[1-S(x)] . \tag{14}$$

With $S(x)=S_{\mathrm{GA}}(x)$, we derive the analytical result[9]

$$g_{\mathrm{GA}}(0)=1-0.846 r_s^{3/4}/C_{23}(r_s) . \tag{15}$$

In the MSA, with $S(x)=S_{\mathrm{MSA}}(x)$, we get

$$g_{\mathrm{MSA}}(0)=1-0.846 r_s^{3/4}/C_{23,0}(r_s) , \tag{16}$$

and in the HFA, with $S(x)=S_0(x)$, we find $g_{\mathrm{HF}}(0)=\frac{1}{2}$.

$g_{\mathrm{MSA}}(0)$ and $g_{\mathrm{GA}}(0)$ versus r_s are shown in Fig. 1. Numerical results for $g_{\mathrm{STLS}}(0)$ (Ref. 3) are shown as solid circles. We find a good agreement between $g_{\mathrm{STLS}}(0)$ and $g_{\mathrm{GA}}(0)$. From general arguments it is clear that $g(0)$ must be positive. For $r_s>3$, $g_{\mathrm{STLS}}(0)$ and $g_{\mathrm{GA}}(0)$ become negative. This negative value for the pair-correlation function for large r_s is a known defect of the STLS approach.[2,3] However, in the STLS approach $g(0)$ is only slightly negative, and the negative value is very small even for very large r_s (see Fig. 1). Similar results have been found for the Bose gas.[9] For the Bose gas one finds (for $r_s\ll 1$) $g(0)=1$ due to the fact that the exchange repulsion is missing in boson systems. For large r_s we find $g_{\mathrm{MSA}}(0)=1-0.846 r_s^{3/4}$. This analytical result corresponds to the large negative values found for $g(0)$ within the RPA.[1,2]

The ground-state energy ε_0 per particle can be expressed as

$$\varepsilon_0(r_s)=\varepsilon_{\mathrm{kin}}(r_s)+\varepsilon_{\mathrm{int}}(r_s) . \tag{17}$$

The kinetic energy is given as $\varepsilon_{\mathrm{kin}}(r_s)/R_y^*=2.2099/r_s^2$,[2]

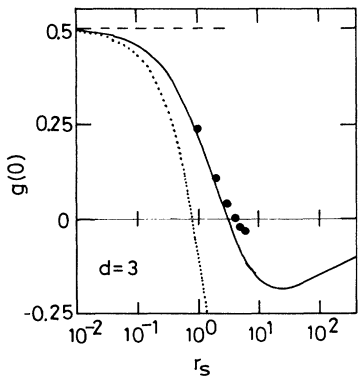

FIG. 1. Pair-correlation function $g_{\mathrm{GA}}(0)$ (solid line) and $g_{\mathrm{MSA}}(0)$ (dotted line) vs RPA parameter r_s for three dimensions according to (15) and (16), respectively. The solid dots represent the STLS results according to Ref. 3.

while the interaction energy is written as[9]

$$\varepsilon_{\rm int}(r_s)/R_y^* = -\frac{1.003\,90}{r_s^2}\int_0^{r_s} dr_s' r_s'^{1/4}/C_{13}(r_s') \ . \tag{18}$$

$R_y^* = 1/2ma^{*2}$ is the effective Rydberg. The correlation energy is defined as $\varepsilon_c(r_s)=\varepsilon_{\rm int}(r_s)-\varepsilon_{\rm ex}(r_s)$. With $C_{13,\rm HF}(r_s)$ we find[2] $\varepsilon_{\rm ex}(r_s)/R_y^* = -0.916\,33/r_s$. Numerically we found $C_{13}(r_s \ll 1) \approx C_{13,\rm HF}(r_s \ll 1)$, and we conclude that $\varepsilon_{\rm int}(r_s \ll 1) \approx \varepsilon_{\rm ex}(r_s \ll 1)$ and $|\varepsilon_{\rm ex}(r_s \ll 1)| \gg |\varepsilon_c(r_s \ll 1)|$. Numerical results for $\varepsilon_{\rm int}(r_s)/\varepsilon_{\rm ex}(r_s)$ versus r_s are shown in Fig. 2 together with numerical results from Refs. 3 and 6. The increase of $\varepsilon_{\rm int}(r_s)/\varepsilon_{\rm ex}(r_s)$ for $r_s > 1$ indicates that correlation effects become important. For small r_s the interaction effects are dominated by the exchange: $\varepsilon_{\rm int}(r_s)/\varepsilon_{\rm ex}(r_s) \approx 1$. In Fig. 2 an analytical result[13] is shown as the dotted line (see Sec. VIII A). In Table II we compare our numerical results for $\varepsilon_c(r_s)$ with the results obtained within the full STLS approach[3] and the Monte Carlo calculations.[6] The agreement is very good up to $r_s \sim 20$. This result indicates that the generalized approximation $G_{\rm GA}(x)$ is a good approximation for treating short-range correlations.

The compressibility κ is given as[3]

$$\frac{\kappa_F}{\kappa} = 1 - 0.166 r_s + 0.0453 r_s^4 \left[\frac{d^2\varepsilon_c}{dr_s^2} - \frac{2}{r_s}\frac{d\varepsilon_c}{dr_s} \right] , \tag{19}$$

with $\kappa_F = 1.706 r_s^5$ as the compressibility of the free-electron gas. With our analytical results for $\varepsilon_c(r_s)$,[14] obtained from the numerical results by a fit, we calculate the compressibility as

$$\kappa_F/\kappa = 0.998 - 0.173 r_s^{1.06} \quad \text{for } 0.1 < r_s < 1 \ , \tag{20a}$$

$$\kappa_F/\kappa = 0.976 - 0.153 r_s^{1.12} \quad \text{for } 1 < r_s < 10 \ , \tag{20b}$$

$$\kappa_F/\kappa = 0.985 - 0.150 r_s^{1.12} \quad \text{for } 10 < r_s < 30 \ . \tag{20c}$$

The result in the HFA is $\kappa_F/\kappa_{\rm HF} = 1 - 0.166 r_s$.

κ_F/κ versus r_s is shown in Fig. 3 together with results obtained in the STLS approach. In the literature, sometimes a negative κ for large r_s has been interpreted to be an instability.[2] However, experimentally there are no indications of such an instability. The physical interpretation is that the positive background charge in the jellium model stabilizes the system (see, for instance, in Refs. 7 and 15).

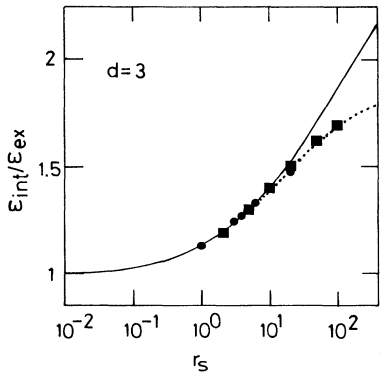

FIG. 2. Solid line: interaction energy $\varepsilon_{\rm int}(r_s)/\varepsilon_{\rm ex}(r_s)$ in units of the exchange energy vs RPA parameter r_s for three dimensions according to (18). The solid dots and solid squares are results from Refs. 3 and 6, respectively. The dotted line corresponds to (58).

TABLE II. Correlation energies ε_c for $d=3$ and various values of r_s: ε_c according to our sum-rule approach, $\varepsilon_{c,\rm STLS}$ according to Ref. 3, and ε_c calculated with ε_0 from Table I of Ref. 6.

r_s	$-\varepsilon_c/R_y^*$	$-\varepsilon_{c,\rm STLS}/R_y^*$ (Ref. 3)	$-\varepsilon_c/R_y^*$ (Ref. 6)
1	0.1200	0.124	0.1195
2	0.0877	0.092	0.0902
3	0.0725	0.075	
4	0.0627	0.064	
5	0.0557	0.056	0.0563
6	0.0503	0.050	
10	0.0372	0.036	0.0372
20	0.0241	0.022	0.0230
50	0.0129		0.0114
100	0.0078		0.0064

The comparison of our results obtained within the sum-rule approach with the exact results[6] and the full STLS approach[3] supports our claim that many-body effects in the three-dimensional electron gas can be described, for $r_s < 20$, by the sum-rule approach.

IV. ELECTRON GAS IN TWO DIMENSIONS

A. Model and theory

In the following we consider an interacting electron gas in two dimensions. The RPA parameter r_s for two-dimensional systems is described as $r_s^2 = 1/\pi N_2 a^{*2}$. The two-dimensional electron density N_2 defines k_F via $N_2 = g_v k_F^2/2\pi$. g_v is the valley degeneracy, and in the following we use $g_v = 1$. The Coulomb-interaction potential in the Fourier space is $V(q) = 2\pi e^2/\varepsilon_L q$. We use dimensionless wave numbers x with $x = q/q_0$. q_0 is expressed as $q_0 = 2/(r_s^{2/3} a^*)$. The SSF of the free-electron gas is given by $S_0(q < 2k_F) = 2[\arcsin(q/2k_F) + q(1 - q^2/$

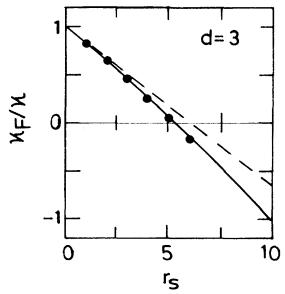

FIG. 3. Solid line: compressibility $\kappa(r_s)$ vs RPA parameter r_s for three dimensions according to (19). The dashed line represents the Hartree-Fock approximation. The solid dots represent results from Ref. 3.

$4k_F^2)^{1/2}/2k_F]/\pi$ and $S_0(q \geq 2k_F)=1$.[4]

Within the STLS approach[9] for two-dimensional systems the LFC is expressed as a one-dimensional q integral over the SSF. One finds the following asymptotic behavior for small and large x: $G(x \ll 1) \propto x$ and $G(x \gg 1)$ is constant.

B. Results

We propose the following GA for the LFC in two dimensions:[9]

$$G_{\mathrm{GA}}(x)=r_s^{2/3}\frac{1.402x}{[2.644C_{12}(r_s)^2+x^2C_{22}(r_s)^2]^{1/2}} . \quad (21)$$

The LFC is described for every r_s by two coefficients $C_{i2}(r_s)$ and $i=1,2$. Coefficients $C_{12}(r_s)$ and $C_{22}(r_s)$ are determined by the nonlinear equations[9]

$$1/C_{12}(r_s)=1.159\,595\int_0^\infty dx[1-S_{\mathrm{GA}}(x)] \quad (22)$$

and

$$1/C_{22}(r_s)=1.426\,348\int_0^\infty dx\, x[1-S_{\mathrm{GA}}(x)] . \quad (23)$$

Equations (22) and (23) can be solved within three approximations as discussed for three dimensions. In the HFA, with $S_{\mathrm{GA}}(x)=S_0(x)$, we find

$$C_{12,\mathrm{HF}}(r_s)=1.436\,78r_s^{1/3} \quad (24a)$$

and

$$C_{22,\mathrm{HF}}(r_s)=2.804\,36r_s^{2/3} , \quad (24b)$$

which results in a LFC of Hubbard type:[4]

$$G_H(q)=\frac{1}{2}\frac{q}{[1.39k_F^2+q^2]^{1/2}} . \quad (25)$$

Using $S_{\mathrm{GA}}(x)=S_{\mathrm{MSA}}(x)$, we find the coefficients in the lowest-order approximation: $C_{12,0}(r_s)$ and $C_{22,0}(r_s)$ with $C_{i2}(r_s \ll 1) \approx C_{i2,0}(r_s \ll 1) \approx C_{i2,\mathrm{HF}}(r_s \ll 1)$.

We calculated $C_{12}(r_s)$ and $C_{22}(r_s)$ by solving (22) and (23). The results are presented in Table III. A systematic study of $C_{12}(r_s)$ and $C_{22}(r_s)$ versus r_s was performed. For large density we find $C_{i2}(r_s \ll 1) \approx C_{i2,\mathrm{HF}}(r_s \ll 1)$; however, see Sec. VIII B. Our numerical results for $C_{12}(r_s)$ and $C_{22}(r_s)$ are described by

$$C_{12}(r_s)=1.135r_s^{0.248} \quad \text{for } 0.1<r_s<1 , \quad (26a)$$

$$C_{12}(r_s)=1.120r_s^{0.216} \quad \text{for } 1<r_s<10 , \quad (26b)$$

$$C_{12}(r_s)=1.127r_s^{0.215} \quad \text{for } 10<r_s<100 \quad (26c)$$

and

$$C_{22}(r_s)=1.687r_s^{0.494} \quad \text{for } 0.1<r_s<1 , \quad (27a)$$

$$C_{22}(r_s)=1.640r_s^{0.530} \quad \text{for } 1<r_s<10 , \quad (27b)$$

$$C_{22}(r_s)=1.314r_s^{0.667} \quad \text{for } 10<r_s<100 . \quad (27c)$$

The accuracy of this fit is about 2%. For large r_s we find $C_{i2,0}(r_s \gg 1)=1$, and our self-consistent equation gives results similar as for bosons $C_{i2,\mathrm{HF}}(r_s) > C_{i2}(r_s) \approx C_{i2,B}(r_s)$.[9]

C. Application

The SSF determines the pair-correlation function $g(r)$.[2] For $r=0$, one finds

$$g(0)=1-2r_s^{2/3}\int_0^\infty dx\, x[1-S(x)] . \quad (28)$$

We conclude that $g(0)$ is determined by $G(x \gg 1)$.

Within the generalized approximation for the LFC we get[9]

$$g_{\mathrm{GA}}(0)=1-1.402r_s^{2/3}/C_{22}(r_s) . \quad (29)$$

In the MSA we derive

$$g_{\mathrm{MSA}}(0)=1-1.402r_s^{2/3}/C_{22,0}(r_s) \quad (30)$$

and in the HFA we find $g_{\mathrm{HF}}(0)=\frac{1}{2}$. $g_{\mathrm{MSA}}(0)$ and $g_{\mathrm{GA}}(0)$ versus r_s is shown in Fig. 4. We find that $g_{\mathrm{GA}}(r=0)$ becomes slightly negative for $r_s>3$: $g_{\mathrm{GA}}(0)>-0.08$. Similar results have been found for the Bose gas.[9] For large r_s we derive the analytical result $g_{\mathrm{MSA}}(0)=1-1.402r_s^{2/3}$. This result explains the large

TABLE III. Parameters for the local-field correction for $d=2$: $C_{12,0}$, $C_{22,0}$, C_{12}, and C_{22} according to (22) and (23) for various values of r_s.

r_s	$C_{12,0}(r_s)$	$C_{22,0}(r_s)$	$C_{12}(r_s)$	$C_{22}(r_s)$
0.01	0.307	0.127	0.308	0.128
0.04	0.475	0.299	0.480	0.311
0.1	0.616	0.486	0.633	0.535
0.4	0.832	0.804	0.913	1.088
1	0.930	0.933	1.123	1.660
4	0.989	0.992	1.509	3.418
10	0.997	0.998	1.844	6.044
40	0.999	0.999	2.497	15.39
100	1.000	1.000	3.037	28.86

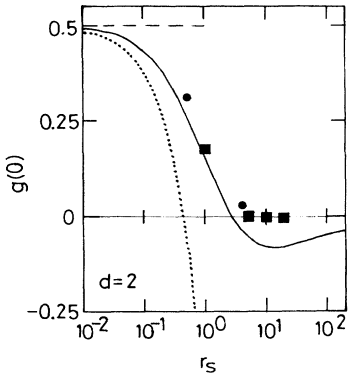

FIG. 4. Pair-correlation function $g_{\mathrm{GA}}(0)$ (solid line) and $g_{\mathrm{MSA}}(0)$ (dotted line) vs RPA parameter r_s for two dimensions according to (29) and (30), respectively. The solid dots represent the STLS results according to Ref. 4. The solid squares represent Monte Carlo results from Ref. 8.

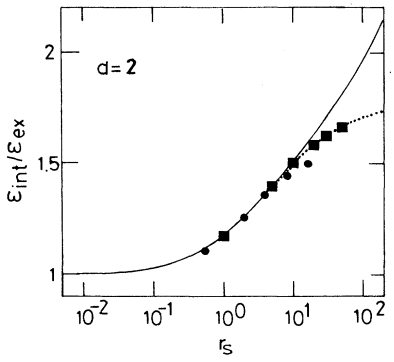

FIG. 5. Solid line: interaction energy in units of the exchange energy $\varepsilon_{int}(r_s)/\varepsilon_{ex}(r_s)$ vs RPA parameter r_s for two dimensions according to (31). The solid dots and solid squares represent results from Refs. 4 and 8, respectively. The dotted line corresponds to (62).

negative values obtained in the RPA for $g(0)$ and large r_s.[4] $g_{STLS}(0)$ (Ref. 4) and Monte Carlo results[8] are shown in Fig. 4 as solid circles and solid squares, respectively.

The correlation energy is defined as in three dimensions as $\varepsilon_c=\varepsilon_{int}-\varepsilon_{ex}$. The kinetic energy is given as $\varepsilon_{kin}(r_s)/R_y^*=1/r_s^2$, while the exchange part is given as[16,17] $\varepsilon_{ex}(r_s)/R_y^*=-1.200\,42/r_s$. Within the generalized approximation for the LFC, we find[9]

$$\varepsilon_{int}(r_s)/R_y^*=-\frac{1.724\,74}{r_s^2}\int_0^{r_s}dr_s' r_s'^{1/3}/C_{12}(r_s')\ . \tag{31}$$

For $r_s<0.01$ we get $\varepsilon_{int}(r_s)/\varepsilon_{ex}(r_s)\approx 1$. $\varepsilon_{int}(r_s)/\varepsilon_{ex}(r_s)$ versus r_s is shown in Fig. 5 together with numerical results from Refs. 4 and 8. The agreement between our results and the results of Ref. 8 is very good up to $r_s=20$. The dotted line represents an analytical result from Ref. 8 (see Sec. VIII B). Numerical results for $\varepsilon_c(r_s)$ are given in Table IV together with the results of the STLS approach[4] and of Monte Carlo calculations (Table I of Ref. 8).

The compressibility is given by

$$\frac{\kappa_F}{\kappa}=1+\frac{r_s^4}{8}\left[\frac{d^2\varepsilon_{int}}{dr_s^2}-\frac{1}{r_s}\frac{d\varepsilon_{int}}{dr_s}\right]\ , \tag{32}$$

TABLE IV. Correlation energies ε_c for $d=2$ and various values of r_s: ε_c according to our sum-rule approach, $\varepsilon_{c,STLS}$ according to Ref. 4, and ε_c according to Table I of Ref. 8.

r_s	$-\varepsilon_c/R_y^*$	$-\varepsilon_{c,STLS}/R_y^*$ (Ref. 4)	$-\varepsilon_c/R_y^*$ (Ref. 8)
1	0.2049	0.211	0.2171
2	0.1528	0.155	
4	0.1067	0.108	
5	0.0938		0.0955
8	0.0702	0.066	
10	0.0607		0.0609
16	0.0441	0.038	
20	0.0377		0.0352
30	0.0283		0.0250
50	0.0194		0.0159

TABLE V. Compressibility κ for a two-dimensional electron gas in units of the compressibility κ_F of the free-electron gas according to (33), together with results in the HFA and Monte Carlo results (Ref. 8).

r_s	κ_F/κ	κ_F/κ_{HF}	κ_F/κ (Ref. 8)
1.0	0.525	0.550	0.528
2.0	0.013	0.100	0.031
3.0	−0.511	−0.350	−0.529

with $\kappa_F=\pi r_s^4/2$ as the compressibility of the free gas. The compressibility in the HFA is $\kappa_F/\kappa_{HF}=1-2^{1/2}r_s/\pi$. With our analytical results for $\varepsilon_c(r_s)$,[14] we calculate the compressibility as

$$\kappa_F/\kappa=\kappa_F/\kappa_{HF}-0.011r_s^{1.83} \quad \text{for } 0.1<r_s<0.5\ , \tag{33a}$$

$$\kappa_F/\kappa=\kappa_F/\kappa_{HF}-0.016r_s^{1.73} \quad \text{for } 0.5<r_s<1\ , \tag{33b}$$

$$\kappa_F/\kappa=\kappa_F/\kappa_{HF}-0.030r_s^{1.53} \quad \text{for } 1<r_s<4\ , \tag{33c}$$

$$\kappa_F/\kappa=\kappa_F/\kappa_{HF}-0.057r_s^{1.35} \quad \text{for } 4<r_s<20\ . \tag{33d}$$

Numerical values for the compressibility for $r_s\le 3$ are given in Table V together with Monte Carlo results taken from a figure in Ref. 8. The agreement between our analytical results and Ref. 8 is very good. We note that correlation effects are already important for $r_s>0.5$; compare with the results in the HFA, which are also given in Table V.

κ_0/κ versus r_s is shown in Fig. 6 together with results obtained for a heterostructure. We note that κ_0/κ is larger in two-dimensional systems with finite width than in the ideally two-dimensional electron gas.

The static response function $\chi(q)$ for the interacting electron gas is expressed as

$$\chi(q)=\chi_0(q)/\{1+V(q)[1-G(q)]\chi_0(q)\}\ , \tag{34}$$

with $\chi_0(q\to 0)=\rho_F$, where ρ_F is the density of states at the Fermi energy. $\chi_0(q)$ is the Lindhard function in two dimensions,[16] and represents the static response function for the free-electron gas: $\chi_0(q<2k_F)/\rho_F=1$ and $\chi_0(q\ge 2k_F)/\rho_F=1-[1-4k_F^2/q^2]^{1/2}$. $\chi(q)$ is shown in

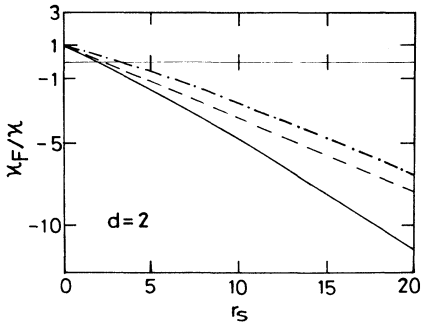

FIG. 6. Solid line: compressibility $\kappa(r_s)$ vs RPA parameter r_s for two dimensions according to (32). The dashed line represents the Hartree-Fock approximation. The dashed-dotted line represents the results for the heterostructure.

Fig. 7 for $r_s=1$ and 5. Very recent numerical results obtained with quantum Monte Carlo simulations[18] in small systems are shown as solid squares. Very good agreement is achieved for $r_s=1$. For $r_s=5$ the agreement is good for small and large wave numbers. However, for $q\sim 2k_F$ our LFC is apparently too small to reproduce the peak in $\chi(q\sim 2k_F)$ and $G(q\sim 2k_F)$ obtained in Ref. 18. Equation (34) defines [with $G(q)=0$] the static response function within the RPA, which is also shown in Fig. 7 as the dashed line.

V. FINITE WIDTH EFFECT IN TWO DIMENSIONS

A. Many-body effects in quantum wells

In the following we present results for the electron gas in two dimensions where the width for the confinement is finite. In order to specify the model we use a quantum well of width L, and infinite barriers for an $Al_xGa_{1-x}As/GaAs/Al_xGa_{1-x}As$ structure with $g_v=1$. For a $Si_{1-x}Ge_x/Si/Si_{1-x}Ge_x$ quantum-well structure the valley degeneracy is $g_v=2$, and our results cannot be applied directly. The interaction potential is written[16] as $V(\mathbf{q},L)=2\pi e^2F(q,L)/\varepsilon_L q$, and $F(q,L)$ is the form factor for the finite width. The form factor for a quantum well was derived in Ref. 19 as

$$F(q,L)=\frac{1}{4\pi^2+q^2L^2}\left[3qL+\frac{8\pi^2}{qL}-\frac{32\pi^4}{q^2L^2}\frac{1-\exp(-qL)}{4\pi^2+q^2L^2}\right] . \quad (35)$$

With $F(q,L=0)=1$ we find for $L=0$ the Coulomb-interaction potential of an ideally two-dimensional electron gas. The behavior for $q\to 0$ is important: $F(q=0,L)=1$.

Within the sum-rule approach the form factor could enter the SSF via $V(q,L)$. However, because $V(q\to 0,L)=V(q)$ we used the same SSF as for an ideally two-dimensional electron gas. We have tested the self-consistent equations in both approximations for the SSF and found that with $V(q,L)=V(q)$ the pair-correlation function was less negative at small electron densities than with $V(q,L)$. In the following we present our results within the approximation: $S_{GA}(q,L)=S_{GA}(q)$. The self-consistent equation for $C_{22}(r_s,L)$ is the same as for the ideally two-dimensional electron gas [see (23)]. For $C_{12}(r_s,L)$ we find

$$1/C_{12}(r_s,L)=1.159\,595\int_0^\infty dx\,[1-S_{GA}(x)]F(xq_0,L) . \quad (36)$$

In Fig. 8 we show the coefficient $C_{12}(r_s,L)/C_{12}(r_s)$ versus L for $r_s=1$, 4, and 10. Decreasing the density ($r_s\to\infty$) leads to $C_{12}(r_s,L)/C_{12}(r_s)\to 1$. In the high-density regime, where k_FL is large, the finite width effects are large. For small density we find $C_{12,HF}(r_s,Lk_F\ll 1)\approx C_{12,HF}(r_s)$, but for large density we get $C_{12,HF}(r_s,Lk_F\gg 1)\gg C_{12,HF}(r_s)$. On the other hand it is clear that $C_{22,HF}(r_s,L)=C_{22,HF}(r_s)$.

In Table VI we give some values for $C_{12}(r_s,L=a^*)$ for different r_s. The finite width reduces many-body effects: $G(q,L)<G(q,L=0)$; compare Table VI with Table III. Unfortunately, Monte Carlo calculations have never been performed for structures with finite L.

In the following we report some results for a quantum well with $L=a^*$. For high density ($k_FL>1$) the Hartree-Fock results depends on the well width, and we find

$$C_{12,HF}(r_s\to 0,L)=0.678L/[a^*r_s^{2/3}\ln(2^{3/2}L/a^*r_s)] \quad (37a)$$

and

$$C_{12,HF}(r_s\to\infty,L)=C_{12,HF}(r_s\to\infty) . \quad (37b)$$

Our numerical results for $C_{12}(r_s,L=a^*)$ are fitted as

$$C_{12}(r_s,L=a^*)=1.135r_s^{0.248} \text{ for } 0.1<r_s<1 , \quad (38a)$$

$$C_{12}(r_s,L=a^*)=1.12r_s^{0.216} \text{ for } 1<r_s<10 , \quad (38b)$$

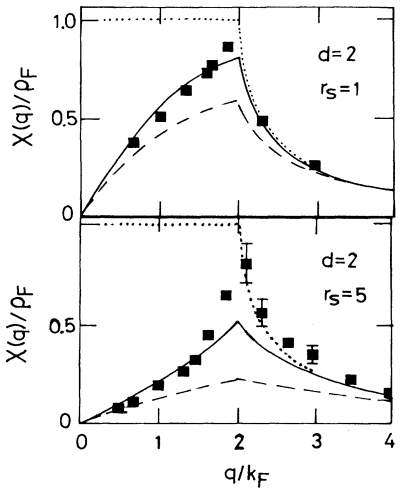

FIG. 7. Solid line: static response function with $\chi(q)$ vs q for $r_s=1$ and 5 and for two dimensions according to (34). The dashed line represents the RPA and the dotted line the free-electron gas. The solid squares correspond to Monte Carlo calculations of Ref. 18.

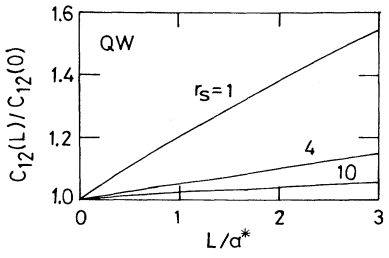

FIG. 8. $C_{12}(r_s,L)/C_{12,0}(r_s)$ vs width L of the quantum well for $r_s=1$, 4, and 10, according to (23) and (36).

TABLE VI. Parameters for the local-field correction for a quantum well (L) and a heterostructure (b) with a form factor: $C_{12}(L)$ and $C_{22}(L)$ according to (23) and (36), and $C_{12}(b)$ and $C_{22}(b)$ according to (23) and (40) for various values of r_s.

r_s	$C_{12}(r_s,L=a^*)$	$C_{22}(r_s,L=a^*)$	$C_{12}(r_s,b)$	$C_{22}(r_s,b)$
0.01	3.25	0.13	1.04	0.13
0.1	1.54	0.52	1.44	0.52
1	1.34	1.62	1.92	1.53
10	1.88	6.02	2.53	5.67
100	3.05	28.85	3.60	28.49

and

$$C_{12}(r_s,L=a^*)=1.127r_s^{0.215} \text{ for } 10<r_s<100 . \quad (38c)$$

The exchange energy is determined by $C_{12,\mathrm{HF}}(r_s,L)$ and, therefore, depends on the width of the well. $r_s\varepsilon_{ex}(r_s,L=a^*)$ versus r_s is shown in Fig. 9 (dashed line) together with the results for an ideally two-dimensional system (solid line). For small densities $|\varepsilon_{ex}|$ in a system with finite width is smaller than in an ideally two-dimensional system.[4] $\varepsilon_c(r_s,L=a^*)$ versus r_s is shown in Fig. 10 (dashed line) together with results for the ideal two-dimensional system (solid line). For given r_s we find that correlation effects are reduced in finite width systems. This result is in agreement with numerical results obtained in the full STLS approach.[4]

B. Many-body effects in heterostructures

For a GaAs/Al_xGa_{1-x}As heterostructure with extension parameter b as $b=(3a^*/44\pi N_2)^{1/3}$, the interaction potential is written as $V(q,b)=2\pi e^2F(q,b)/\varepsilon_L q$, with[16]

$$F(q,b)=\frac{1}{(1+qb)^3}[1+\tfrac{8}{9}qb+\tfrac{1}{3}q^2b^2] . \quad (39)$$

In this model we used a vanishing depletion density N_D. For a finite depletion density the extension parameter b is somewhat modified. $b=0$ corresponds to the ideally two-dimensional electron gas.

The self-consistent equation for $C_{22}(r_s,b)$ is the same as for the ideally two-dimensional electron gas [see (23)].

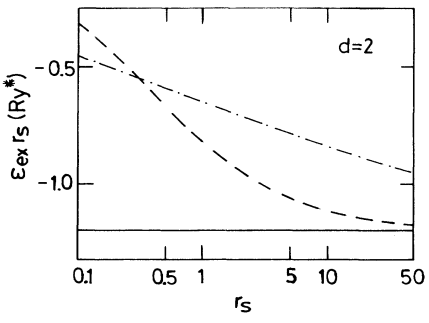

FIG. 9. Exchange energy $r_s\varepsilon_{ex}(r_s)$ vs RPA parameter r_s for two dimensions (solid line), for a quantum well with $L=a^*$ (dashed line), and for a heterostructure (dashed-dotted line).

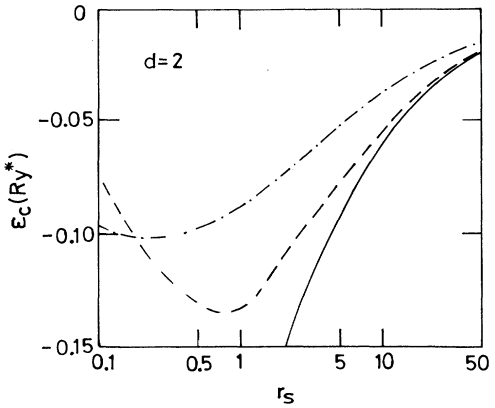

FIG. 10. Correlation energy $\varepsilon_c(r_s)$ vs RPA parameter r_s for two dimensions (solid line), for a quantum well with $L=a^*$ (dashed line), and for a heterostructure (dashed-dotted line).

For $C_{12}(r_s,b)$, we find

$$1/C_{12}(r_s,b)=1.159\,595\int_0^\infty dx[1-S_{\mathrm{GA}}(x)]F(xq_0,b) . \quad (40)$$

We realize that $q_0b=(\frac{6}{11})^{1/3}$ is independent of r_s. Therefore, the coefficients $C_{i2}(r_s,b)$ are universal and depend only on r_s. Numerical results for $C_{12}(r_s,b)$ are given in Table VI for different values of r_s. By comparing Tables III and VI, it is clearly seen that $G(q)$ is reduced by the finite width of the electron gas.

For the Hartree-Fock result, we find

$$C_{12,\mathrm{HF}}(r_s\to 0,b)=6.2/\ln(1/r_s) \quad (41a)$$

and

$$C_{12,\mathrm{HF}}(r_s\to\infty,b)=C_{12,\mathrm{HF}}(r_s\to\infty) . \quad (41b)$$

The numerical results for $C_{12}(r_s)$ are expressed as

$$C_{12}(r_s,b)=1.914r_s^{0.119} \text{ for } 0.1<r_s<10 \quad (42a)$$

and

$$C_{12}(r_s,b)=1.764r_s^{0.154} \text{ for } 10<r_s<100 . \quad (42b)$$

With $C_{12,\mathrm{HF}}(r_s,b)$, we calculate the exchange energy as

$$\varepsilon_{ex}(b)=-0.649/r_s^{0.858} \text{ for } 0.3<r_s<3 \quad (43a)$$

and

$$\varepsilon_{ex}(b)=-0.694/r_s^{0.920} \text{ for } 3<r_s<100 . \quad (43b)$$

$r_s\varepsilon_{ex}(r_s,b)$ versus r_s is shown in Fig. 9 (dashed-dotted line) together with the results for a quantum well (dashed line). For small density the width effect is small; however, for large density $|\varepsilon_{ex}|$ is smaller than for the ideally two-dimensional system.

The correlation energy is expressed as

$$\varepsilon_c(b)=-0.0895/r_s^{0.116} \text{ for } 0.3<r_s<1 , \quad (44a)$$

$$\varepsilon_c(b)=-0.0889/r_s^{0.279} \text{ for } 1<r_s<3 , \quad (44b)$$

$$\varepsilon_c(b) = -0.1084/r_s^{0.455} \quad \text{for } 3 < r_s < 10 , \tag{44c}$$

$$\varepsilon_c(b) = -0.157/r_s^{0.612} \quad \text{for } 10 < r_s < 70 . \tag{44d}$$

$\varepsilon_c(r_s,b)$ versus r_s for the heterostructure is shown in Fig. 10. The finite width reduces the correlation energy for large density if compared to the ideally two-dimensional electron gas. We note, however, that the ratio $\varepsilon_{\rm int}(r_s,b)/\varepsilon_{\rm ex}(r_s,b)$ is nearly the same as for the ideally two-dimensional system. This means that in a structure with finite width correlation effects become important at a similar electron density as for a structure with zero width.

The compressibility of the heterostructure is written as

$$\kappa_F/\kappa(b) = 1 - 0.20 r_s^{1.14} - 0.0028 r_s^{1.88} \quad \text{for } 0.3 < r_s < 1 , \tag{45a}$$

$$\kappa_F/\kappa(b) = 1 - 0.12 r_s^{1.14} - 0.0071 r_s^{1.72} \quad \text{for } 1 < r_s < 3 , \tag{45b}$$

$$\kappa_F/\kappa(b) = 1 - 0.23 r_s^{1.08} - 0.015 r_s^{1.55} \quad \text{for } 3 < r_s < 10 , \tag{45c}$$

$$\kappa_F/\kappa(b) = 1 - 0.23 r_s^{1.08} - 0.031 r_s^{1.39} \quad \text{for } 10 < r_s < 70 . \tag{45d}$$

The first two terms on the right-hand side of Eqs. (45) represent the HFA. We find for a heterostructure that $\kappa_F/\kappa(b) < 0$ for $r_s > 3.5$.

VI. PLASMON DISPERSION

The plasmon dispersion $\omega_p(q)$ in the RPA with a finite LFC is given by[1]

$$1 + V(q)[1 - G(q)]\chi_0[\omega_p(q), q] = 0 . \tag{46}$$

For $G(q) = 0$, one obtains the plasmon dispersion in the RPA. In the following we show that for $r_s > 1$ the finite LFC strongly modifies the plasmon dispersion. We compare with results obtained in Refs. 3 and 4.

A. Rotons in three dimensions: $r_s > 5$

For small wave numbers the plasmon dispersion is given by

$$\omega_p(q) = \omega_{p0}\{1 + 0.368 r_s (qa^*)^2 [1 - 0.138 r_s C_{13,\rm HF}(r_s)/C_{13}(r_s)]\} , \tag{47}$$

with $\omega_{p0} = \omega_p(q=0) = (4\pi N_3 e^2/\varepsilon_L m)^{1/2}$. The term in (47) containing C_{13} represents the reduction of the plasmon energy by the finite LFC. For small r_s the prefactor of the q^2 term is positive. However, for large r_s this prefactor becomes negative. For $1 = 0.138 r_s C_{13,\rm HF}(r_s)/C_{13}(r_s)$, the q^2 term vanishes. With $C_{13}(r_s=7) = 1.2$ and $C_{13,\rm HF}(r_s=7) = 1.8$, we derive $r_{sr} \sim 4.8$. For $r_s > r_{sr}$ we predict a roton structure in the plasmon dispersion. Indeed, such a roton structure is well known in the three-dimensional electron gas from the STLS approach.[3]

The plasmon dispersion for $r_s = 20$ is shown in Fig. 11 together with the RPA and STLS results.[3] At $q = q_{\rm EH}$ the plasmon mode enters the particle-hole spectrum. We mention that $q_{\rm EH}$ is strongly reduced due to the LFC if compared with the result in the RPA. $q_1 = 0$ and q_2 for $r_s > r_{sr}$ describe the point in the dispersion relation where $d\omega_p(q)/dq = 0$. We conclude for q_2 that the density of plasmon modes is singular. A systematic study of $q_2 a^*$ and $q_{\rm EH}/k_F$ versus r_s is given in Table VII. We believe that the large density of plasmon modes at q_2 can be measured in doped semiconductors at (very) low temperatures.

B. Rotons in two dimensions: $r_s > 45$

For small wave numbers the plasmon dispersion is given by

$$\omega_p(q) = \omega_{p0}\{1 + 0.375 qa^* [1 - 0.392 r_s C_{12,\rm HF}(r_s)/C_{12}(r_s)]\} , \tag{48}$$

with $\omega_{p0} = \omega_p(q \to 0) = (2\pi N_2 e^2 q/\varepsilon_L m)^{1/2}$. The term in (48) containing C_{12} represents the reduction of the plasmon energy by the finite LFC due to exchange and correlation. For small r_s the coefficient of the qa^* term is positive. However, for small density $1 < 0.392 r_s C_{12,\rm HF}(r_s)/C_{12}(r_s)$ this term becomes negative. We conclude that for $r_s > 2.5$ exchange and correlation effects are very important for the plasmon dispersion in two-dimensional systems. Note, however, that $r_s > 2.5$ does not correspond to a roton structure due to the fact that in (48) $\omega_p(q \to 0) \propto q^{1/2}$ increases with increasing wave number.

In Fig. 12 the plasmon energy $\omega_p(q)$ versus q is shown for $r_s = 10$, 20, and 40. The dotted lines correspond to the RPA. For finite wave numbers $q > 0.2 k_F$, a large difference is found between the plasmon dispersion calculated in the RPA and calculated with the finite LFC. At $q = q_{\rm EH}$ the plasmon mode enters the electron-hole spectrum. The values $q_{\rm EH}$ calculated within our theory are much smaller than within the RPA. For $r_s = 10$, 20, and 40, we find $q_{\rm EH} = 1.57 k_F$, $1.80 k_F$, and $2.04 k_F$, respectively. The corresponding numbers in Ref. 20 are $q_{\rm EH} = 1.5 k_F$, $1.75 k_F$, and $1.85 k_F$.

In a two-dimensional electron gas a roton structure has been predicted for $r_s \geq 40$.[20] For $r_s = 50$, not shown in Fig. 12, a maximum of the plasmon energy is found at $q_1 = 1.035 k_F$ with $\omega_p(q_1) = 7.160 \varepsilon_F$, and a minimum of the plasmon energy at $q_2 = 1.280 k_F$ with $\omega_p(q_2)$

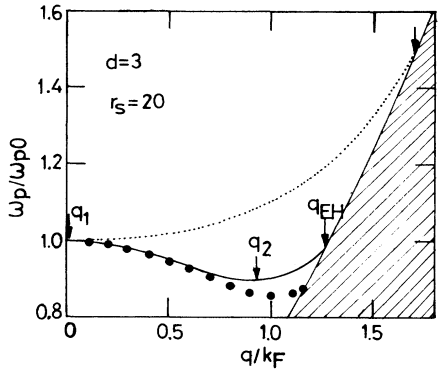

FIG. 11. Solid line: plasmon energy ω_p vs wave number q for $r_s=20$ according to (46) for three dimensions. The dotted line represents the RPA result. The shaded area represents the particle-hole spectrum. q_{EH} represents the wave number where the plasmon mode enters the particle-hole spectrum. The solid dots are numerical results within the full STLS approach (Ref. 3).

$=7.147\varepsilon_F$. This structure is interpreted as a roton structure similar to the roton structure of superfluid helium. In a recent paper roton behavior in the plasmon dispersion of interacting bosons in two dimensions was found for $r_s>30$.[9] For $r_s<45$ a roton structure is absent. However, the LFC has a substantial effect on the plasmon dispersion for $q/k_F>0.2$ (see Fig. 12). The main effect is that the density of plasmon modes in this q range is strongly enhanced compared to the density of plasmon modes for $G(q)=0$; with a finite LFC, $dq/d\omega_p(q)$ is much larger than for $G(q)=0$.

The comparison between our results and the results from Refs. 20 (Monte Carlo) and 4 (STLS) is shown in Fig. 13. For $q<k_F$ the reduction of the plasmon energy due to the LFC is determined by $C_{12}(r_s)$. Our values for $C_{12}(r_s)$ are somewhat smaller than the $C_{12}(r_s)$ obtained within the Monte Carlo calculations,[8] which are input parameters in Ref. 20. For instance, we obtain $C_{12}(r_s=5)=1.58$, $C_{12}(r_s=10)=1.84$, $C_{12}(r_s=20)=2.15$, and $C_{12}(r_s=40)=2.50$, while the Monte Carlo parameters, from $G(q)$ given in Ref. 20, are determined as $C_{12}(r_s=5)=1.71$, $C_{12}(r_s=10)=1.98$, $C_{12}(r_s=20)=2.44$, and $C_{12}(r_s=40)=3.01$. Smaller values for $C_{12}(r_s)$ indicate a larger effect of the LFC and, therefore, a smaller plasmon energy. This is shown in Fig. 13 for

TABLE VII. Parameters for the plasmon dispersion in three dimensions for various RPA parameters r_s (see Fig. 11).

r_s	$\omega_{p0}(R_y^*)$	$\omega_p(q_2)/\omega_{p0}$	q_2/k_F	q_2a^*	q_{EH}/k_F
5	0.310	0.999	≈ 0	≈ 0	0.86
6	0.236	0.995	0.32	0.101	0.94
7	0.187	0.992	0.43	0.118	0.98
8	0.153	0.984	0.52	0.124	1.01
10	0.110	0.968	0.63	0.121	1.08
15	0.060	0.927	0.82	0.105	1.19
20	0.039	0.893	0.93	0.089	1.27

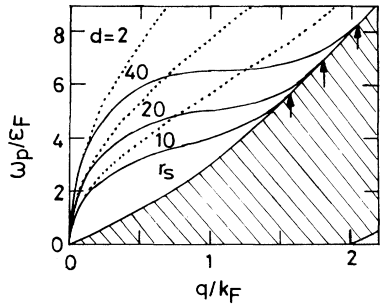

FIG. 12. Solid lines: plasmon energy ω_p vs wave number q for $r_s=10$, 20, and 40 for two dimensions according to (46). The dotted lines represent the RPA results. The shaded area represents the particle-hole spectrum. The arrows indicate q_{EH}.

$r_s=20$. The plasmon energy for $r_s=16$, for large wave numbers, is about 5% larger than the plasmon energy obtained in the STLS approach.[4] Of course, the difference between our results and the exact results for the LFC and the plasmon dispersion becomes smaller for decreasing r_s.

VII. INSTABILITY IN LAYERED STRUCTURES

A charge-density-wave (CDW) instability has been discussed for electronic double-quantum-well structures.[21] In a recent paper we argued that exchange and correlation effects induce a CDW instability in all layered quantum liquids of fermions and bosons.[22] We described the effect by a finite LFC, and discussed Fermi quantum liquids with exchange and Bose quantum liquids with correlation. In the following we apply the LFC calculated within the sum-rule version of the STLS approach to give more accurate results for the instability point for electrons in a double-plane structure, now including correlation effects.

For two layers with distance α, the static susceptibility $\chi_\pm(q)$ is written as[21]

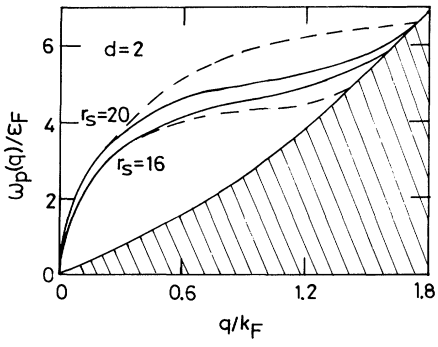

FIG. 13. Solid lines: plasmon energy ω_p vs wave number q for $r_s=16$ and 20 for two dimensions according to (46). The dashed lines represent results from Ref. 20 for $r_s=20$ and from Ref. 4 for $r_s=16$. The shaded area represents the particle-hole spectrum.

$$\chi_{\pm}(q)=\frac{\chi_0(q)}{1+\{V(q)[1-G(q)]\pm V_{12}(q)\}\chi_0(q)} , \quad (49)$$

with $V_{12}(q)=V(q)\exp(-q\alpha)$ as the interlayer Coulomb-interaction potential, and $V(q)=2\pi e^2/\varepsilon_L q$ the intralayer Coulomb-interaction potential. For a two-layer system two plasmon modes exist. The two plasmon modes correspond to in-phase and out-of-phase oscillations of the two layers.

The CDW instability is characterized by $1/\chi_-(q=q_c\geq 0)=0$ (Ref. 21) or $\omega_{p-}(q=q_c\geq 0)=0$.[22] For the critical distance α_c, we find[22]

$$\alpha_c/a^*=\frac{0.431 r_s^{4/3}}{C_{12}(r_s)}-0.5 . \quad (50)$$

For $\alpha>\alpha_c$ the electron gas is stable, and for $\alpha<\alpha_c$ we find an instability of the electron gas. In the HFA we derive[22]

$$\alpha_{c,\mathrm{HF}}/a^*=0.30 r_s-0.5 . \quad (51)$$

Because of $C_{12}(r_s)<C_{12,\mathrm{HF}}(r_s)$ we conclude that the correlation effects increase α_c compared to the result in the HFA. For small r_s correlation effects are unimportant, and α_c is determined by exchange effects. From the strong-coupling results[8] for the correlation energy [determined by $C_{12}(r_s)$] we conclude that for large r_s the enhancement of α_c by correlation effects is given by a factor of about 2.

For $r_s=10$ and 20, with (50) we obtain $\alpha_c=4.53a^*$ and $10.4a^*$, respectively. The corresponding values found numerically in Ref. 21 for two quantum wells with a finite width L are $\alpha_c=4.7a^*$ (for $L=100$ Å) and $9.6a^*$ (for $L=200$ Å). We note that a dependence of α_c on the occupation number was discussed in Ref. 21. In our theory we used the Fermi-Dirac occupation. The value $\alpha_c=4.7a^*$ (for $L=100$ Å) for $r_s=10$ represents the Fermi-Dirac occupation. With the Monte Carlo occupation a critical distance $\alpha_c=3.2a^*$ (for $L=100$ Å) for $r_s=10$ was reported in Ref. 21.

The results for α_c/a^* versus r_s according to (50) and (51) are shown in Fig. 14. The instability region is increased by correlation effects. The numerical results according to (50) and shown in Fig. 14 can be approximated by

$$\alpha_c/a^*=0.24 r_s^{1.25} . \quad (52)$$

For fixed α the critical RPA parameter r_{sc} defines the critical electron density N_{2c}. Equation (52) can be rewritten in terms of the critical electron density as $N_{2c}\alpha^2=0.10[\alpha_c/a^*]^{0.4}$.

The static susceptibility $\chi_-(q)$ becomes singular for $x_c=q_c/q_0$. With (49), x_c is given by

$$x_c=r_s^{2/3}[G(x_c)+\exp(-2x_c\alpha/a^* r_s^{2/3})-1]\chi_0(x_c)/\rho_F . \quad (53)$$

We note that $k_F=q_0/(2^{1/2}r_s^{1/3})$. Numerical values for q_c versus α for $r_s=10$ are shown in Fig. 15. We find a small region with two solutions $q_{c\pm}$. $q_{c-}=0$ corresponds to α_c according to (50). For $q_{c,m}\equiv q_{c+}=q_{c-}$ (see Fig. 15), α exhibits a maximum $\alpha_{c,m}$; we find $\alpha_{c,m}=5.25a^*$ and $\alpha_c=4.53a^*$ for $r_s=10$. $\alpha_{c,m}$ defines the stability regime of the Fermi liquid, and some numerical values are shown in Fig. 14 as solid dots. With Fig. 14 it is clear that (50) is an excellent analytical expression for the instability.

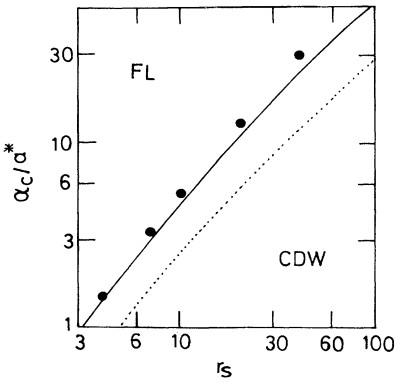

FIG. 14. Critical layer distance α_c vs RPA parameter r_s. The solid line corresponds to (50). The dotted line represents the results in the HFA [(51)]. The stability region for the Fermi liquid (FL) and the instability region for the charge-density wave (CDW) are indicated. Numerical results for $\alpha_{c,m}$ according to (53) are shown as solid dots.

Our analytical result in (50) was derived within the assumption that $q_c/q_0\ll 1$. Indeed, in Fig. 15 we see that the instability already occurs for $\alpha_{c,m}>\alpha_c$. However, for $q_{c,m}/q_0\ll 1$ our analytical result for α_c is a very good approximation. Similar results have been found for boson double-layer structures.[9] For $r_s=10$ we notice that $q_{c,m}=0.9k_F$. For $r_s=20$ we find $\alpha_{c,m}=12.8a^*$ and $\alpha_c=10.29a^*$, and the critical wave number is $q_{c,m}=1.14k_F$. $q_{c,m}/k_F$ versus r_s is shown in Fig. 16, and we conclude that $q_{c,m}<2k_F$.

Finally, we discuss the behavior of q_c for $\alpha=0$. For $\alpha\to 0$ with (53) and for $q_L=q_c(\alpha=0)$, we find

$$x_L=r_s^{2/3}G(x_L)\chi_0(x_L)/\rho_F . \quad (54)$$

For $q_L\gg 2k_F$, we derive the analytical result

$$\frac{q_L}{k_F}=r_s^{5/9}\frac{1.582}{C_{22}^{1/3}} , \quad (55)$$

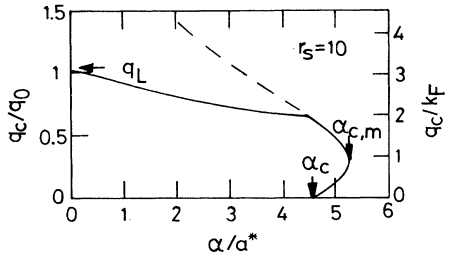

FIG. 15. Solid line: q_c vs α for $r_s=10$ according to (53). The arrow for α_c indicates the analytical solution according to (50). The dashed line corresponds to (53), with $\chi_0(0\leq q<\infty)=\rho_F$.

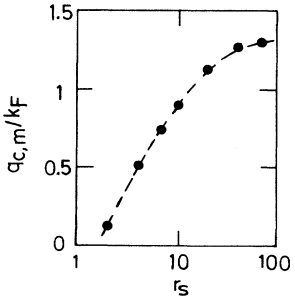

FIG. 16. Solid dots: $q_{c,m}$ vs r_s according to (53). The dashed line is a guide to the eye.

and in the HFA (55) corresponds to $q_{L,\mathrm{HF}}/k_F=1.12r_s^{1/3}$. For $r_s=10$ with (55), we obtain $q_L=3.12k_F$, and this value is in good agreement with our numerical result shown in Fig. 15. With (55) we conclude that for large r_s, $q_L>2k_F$. For $q_L\leq 2k_F$ we argue that q_L is defined by $x_L=r_s^{2/3}G(x_L)$.

VIII. CORRELATIONS FOR $r_s<1$

While the kinetic and exchange parts of the ground-state energy are given as analytical results, at least for the three- and ideally two-dimensional electron gases, the correlation energy is more difficult to calculate. For $r_s<1$ the correlation effects are small if compared with the exchange and kinetic energies. In all applications of the STLS approach to the interacting electron gas the regime $r_s>0.5$ has been studied. While in ordinary metals the $1<r_s<10$ regime is the most important, doped semiconductors in two and three dimensions appear in general in the $0.1<r_s<3$ regime. It was recently found that quantum effects are important in white dwarfs with $0.001<r_s<0.01$.[23] Therefore, we believe that a systematic study of the correlation effects within the STLS approach for $r_s<1$ is an important issue.

However, is it really possible to compare the results obtained in the sum-rule version of the STLS approach with exact results[24] available for the correlation energy for $r_s\to 0$? We used an analytical expression for the SSF, and it is not evident that this approximation gives good results for the correlation for $r_s\ll 1$. For $r_s\ll 1$ the calculation of ε_c becomes numerically difficult because of $\varepsilon_{\mathrm{int}}\sim\varepsilon_{\mathrm{ex}}$ and $\varepsilon_c=\varepsilon_{\mathrm{int}}-\varepsilon_{\mathrm{ex}}\ll\varepsilon_{\mathrm{int}}$. It is this numerical problem which did not allow calculations in the high-density limit within the STLS approach within a limited computer time (see Refs. 3 and 4). In the sum-rule version this numerical problem is less expensive. In the following we present some results for ε_c for $0.001<r_s<1$. In order to obtain ε_c for $r_s>0.001$ we used the self-consistently calculated $C_{12}(r_s)$ and $C_{13}(r_s)$ for $r_s>1\times10^{-5}$.

A. Correlation in three dimensions

The correlation energy in three dimensions is given by

$$\varepsilon_c(r_s)/R_y^*=-\frac{0.916}{r_s^2}\int_0^{r_s}dr_s'\frac{C_{13,\mathrm{HF}}(r_s')-C_{13}(r_s')}{C_{13}(r_s')}\ . \tag{56}$$

We note that $C_{13,\mathrm{HF}}(r_s)-C_{13}(r_s)$ must be calculated very accurately in order to get reliable numbers for the correlation energy. Note that the factor $1/r_s^2$ in (56) is 10^4 for $r_s=0.01$, while $\varepsilon_c(r_s=0.01)/R_y^*\sim-0.3$ and $C_{13}(r_s=0.01)\sim 0.3$. This analysis clearly shows that $C_{13}(r_s)$ must be calculated with high accuracy. We add that in order to calculate $\varepsilon_c(r_s)$ the coefficients $C_{13}(r_s)$ are determined more precisely than in Table I.

Numerically, for $r_s\ll 1$ we find

$$C_{13}(r_s)=C_{13,\mathrm{HF}}(r_s)\{1+b_1r_s[2\ln(r_s)+1]-2b_2r_s\}\ . \tag{57}$$

With (56) the correlation energy is expressed as $\varepsilon_c(r_s\ll1)/R_y^*=0.916[b_1\ln(r_s)-b_2]$. Using $r_s=5\times10^{-3}$ and 1×10^{-2}, from our numerical results for $C_{13}(r_s)$ we obtain the parameters $b_1=0.062$ and $b_2=0.14$. For the correlation energy we find $\varepsilon_c(r_s\ll1)/R_y^*=0.057\ln(r_s)-0.13$. Indeed, such a power series for the three-dimensional electron gas was derived by Gell-Mann and Brueckner:[24] $\varepsilon_c(r_s\ll1)/R_y^*=0.0622\ln(r_s)-0.094$.

Following earlier work an analytical expression for the correlation energy in the full density ($0<r_s<100$) range was proposed very recently[13] as

$$\varepsilon_c(r_s)/R_y^*=-4\kappa_1(1+\kappa_2r_s)\ln\left[1+\frac{1}{2\kappa_1(\beta_1r_s^{1/2}+\beta_2r_s+\beta_3r_s^{3/2}+\beta_4r_s^2)}\right]\ , \tag{58}$$

with $\kappa_1=0.031\,09$, $\kappa_2=0.213\,70$, $\beta_1=7.5957$, $\beta_2=3.5876$, $\beta_3=1.6382$, and $\beta_4=0.492\,94$. The asymptotic laws, derived with (58), are written as[13]

$$\varepsilon_c(r_s)/R_y^*=0.0622\ln(r_s)-0.0932+0.013\,28r_s\ln(r_s)-0.020\,86r_s \tag{59a}$$

for $r_s\ll1$, and

$$\varepsilon_c(r_s)/R_y^*=-0.867/r_s+2.8816/r_s^{3/2} \tag{59b}$$

for $r_s\gg1$. We conclude that $\varepsilon_{\mathrm{int}}(r_s)/\varepsilon_{\mathrm{ex}}(r_s)=1.95$ for $r_s\gg1$ (see Fig. 2).

We compared the correlation energy obtained for the three-dimensional electron gas within the sum-rule approach with the analytical result (58). We found perfect agreement ($<1\%$ deviation) for $0.01<r_s<1$. For $0.0001<r_s<0.004$ our numerical results are about 5% larger than the analytical result according to (59a).

The good agreement of the correlation energy according to (58) with our numerical results supports our claim

that the sum-rule version of the STLS approach can be used to obtain the ground-state energy even for $0.001 < r_s < 1$. Indeed, this was never demonstrated in the literature for the large density range. For $r_s > 1$ we have already compared the correlation energy within the sum-rule approach with the Monte Carlo[6] results in Table II and Fig. 2, and we found good agreement for $r_s < 20$. We conclude that the sum-rule version of the STLS approach gives quantitatively correct results for the correlation energy for $0.001 < r_s < 20$. For $r_s > 3$, we suggest a one-sum-rule approach in Sec. IX.

B. Correlation in two dimensions

For two dimensions the correlation energy is expressed as

$$\varepsilon_c(r_s)/R_y^* = -\frac{1.2004}{r_s^2}\int_0^{r_s} dr_s' \frac{C_{12,\mathrm{HF}}(r_s')-C_{12}(r_s')}{C_{12}(r_s')} . \tag{60}$$

We mention again that $C_{12}(r_s)$ was calculated more precisely than indicated in Table III. We also note that for all r_s studied ($0.001 < r_s < 200$) we found $C_{12,\mathrm{HF}}(r_s) > C_{12}(r_s)$. We conclude with (60) that $\varepsilon_c(r_s) < 0$, in agreement with general arguments.[1]

From our numerical results, for $r_s \ll 1$ we derive

$$C_{12}(r_s) = C_{12,\mathrm{HF}}(r_s)[1 - b_3 r_s] . \tag{61}$$

With (60) we conclude that $\varepsilon_c(r_s=0) = -0.60 b_3$. For $r_s = 3\times 10^{-3}$, with $C_{12,0}$ we obtain $b_3 = 0.93$ and $\varepsilon_c(r_s=0)/R_y^* = -0.555$. However, with C_{12} we find $b_3 = 0.64$ and $\varepsilon_c(r_s=0)/R_y^* = -0.385$. This calculation clearly shows that for $r_s = 3\times 10^{-3}$ the finite LFC in the expression for the SSF is still important for the calculation of ε_c. We conclude that even for $r_s \to 0$ the finite LFC is important for a correct determination of the correlation energy. Within the STLS approach this is quite a surprising fact: one could believe that the LFC is unimportant for a small RPA parameter. For the correlation energy we have shown that this is not the case.

For the ideally two-dimensional electron gas the expression

$$\varepsilon_c(r_s)/R_y^* = a_0 \frac{1 + a_1 r_s^{1/2}}{1 + a_1 r_s^{1/2} + a_2 r_s + a_3 r_s^{3/2}} \tag{62}$$

was given in Ref. 8 with $a_0 = -0.3568$, $a_1 = 1.1300$, $a_2 = 0.9052$, and $a_3 = 0.4165$. For $r_s \to 0$ one gets from (62) that $\varepsilon_c(r_s \to 0)/R_y^* = -0.3568$, which is near to the predicted values $\varepsilon_c(r_s \to 0)/R_y^* = -0.38$ (Ref. 25) and -0.39.[26–28] For $r_s \to 0$ the analytical result

$$\varepsilon_c(r_s)/R_y^* = -0.38 - 0.172 r_s \ln(r_s) \tag{63}$$

was given in Ref. 25. For small density, (62) implies $\varepsilon_c(r_s) = -0.986/r_s$ and $\varepsilon_{\mathrm{int}}(r_s)/\varepsilon_{\mathrm{ex}}(r_s) = 1.81$ for $r_s \gg 1$ (see Fig. 5). In connection with the CDW instability in Sec. VIII, we interpreted this factor 1.81 as a factor 2 for the enhancement due to correlations.

In Fig. 17 we have shown our calculated correlation energy ε_c versus r_s for $0.001 < r_s < 1$ and for two dimensions. Equations (62) and (63) are shown as the dashed and dotted lines, respectively. Our numerical results for $0.001 < r_s < 1$ are in good agreement with (62). For $r_s > 1$ we have compared the results of the sum-rule approach with the Monte Carlo calculations[8] in Table III and Fig. 5, and we found good agreement for $r_s < 20$. On the other hand, we conclude that the analytical expression for ε_c, as proposed in Ref. 29 for $r_s > 2^{1/2}$, is not in agreement with the Monte Carlo results.

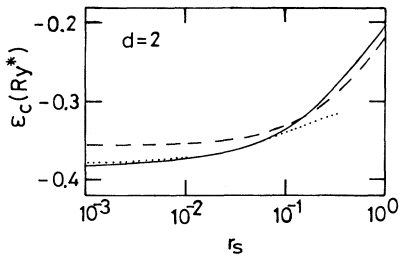

FIG. 17. Solid line: correlation energy $\varepsilon_c(r_s)$ vs RPA parameter r_s for two dimensions. The dashed line represents the analytical result according to (62), and the dotted line represents (63).

IX. SIMPLIFIED APPROACH FOR $r_s > 3$

In two dimensions we found for $r_s > 3$ a small negative pair-correlation function. This means that the effective potential $V_{\mathrm{eff}}(q \to \infty) = V(q \to \infty)[1 - G(q \to \infty)]$ is negative for $r_s > 3$ and large wave numbers. In some calculations, where the LFC enters, this defect in the theory might be acceptable; for instance, for q integrals over the dielectric function containing the LFC. However, it is clear that in other calculations, where one directly uses $G(q)$, this behavior of the LFC might be unacceptable. A possible solution for this problem is to determine $C_{22}(r_s)$ in such a way that $g(0) = 0$, and to use the one-sum-rule version of the STLS approach to determine $C_{12}(r_s)$.

With the sum-rule approach and using $C_{22,g}(r_s) = 1.402 r_s^{2/3}$ for two dimensions, which leads to $G(q \to \infty) = 1$ and $g(0) = 0$, we find the coefficient $C_{12,g}(r_s)$, calculated with (22), numerically similar to the full two-sum-rule approach (compare Tables VIII and III). Of course, this one-sum-rule approximation can only be applied for $r_s > 3$, where the Monte Carlo results

TABLE VIII. Parameters $C_{12,g}(r_s)$ for two dimensions and $C_{13,g}(r_s)$ for three dimensions calculated within the one-sum-rule approximation for small wave numbers with $G(q \to \infty) = 1$ and $g(0) = 0$.

r_s	$C_{12,g}(r_s)$	$C_{13,g}(r_s)$
4	1.570	1.106
10	1.897	1.229
40	2.596	1.447
100	3.280	1.644

indicate a very small value for $g(0)$. For $r_s<3$ where $G(q\rightarrow\infty)<1$, the two-sum-rule version of the STLS approach must be used.

For three dimensions and for $r_s>3$, we use $C_{23,g}(r_s)=0.846r_s^{3/4}$, corresponding to $G(q\rightarrow\infty)=1$ and $g(0)=0$, and we solve this with Eq. (8). Some results for $C_{13,g}(r_s)$ are given in Table VIII and are numerically very similar to the values calculated within the two-sum-rule approach (compare Tables I and VIII).

We conclude that for $r_s\geq 3$ the one-sum-rule approach is a very useful approximation if the condition $G(q\rightarrow\infty)=1$, resulting in $g(0)=0$, is necessary. We mention that a discussion such as performed in this section cannot be performed in the full STLS approach, because there one does not work with an analytical form of the LFC. The numerical values of the coefficients $C_{13,g}(r_s)$ and $C_{12,g}(r_s)$ do not change much compared to $C_{13}(r_s)$ and $C_{12}(r_s)$, respectively, derived within the two-sum-rule approach. Therefore, we argue that for $r_s>20$ the correlation energy is not in agreement with the Monte Carlo results. On the other hand, we believe that this defect of our theory might in fact not be a strong limitation to applications; for dynamical effects it is much more important that $G(q)\leq 1$, in order to avoid artificial singularities. We want to mention that for large r_s, $G(q\sim 2.5k_F)>1$ (see Ref. 20). This behavior cannot be described by our approach.

X. DISCUSSION

It is known that the STLS approach is not exact; the pair-correlation function $g(r)$ for $r=0$ is negative for large values of r_s. However, in the STLS approach $g(r=0)$ is only slightly negative, even for very large r_s as was shown in this paper. The frequency dependence of the LFC was also neglected in the STLS approach. In Ref. 20 a theory for the dynamical behavior of the repulsion hole in the interacting electron gas was developed. However, this theory uses the static LFC calculated within the Monte Carlo approach as *input*. Therefore, we believe that an efficient method to calculate the LFC is useful. Backflow corrections[1] are also neglected in the STLS approach and in our sum-rule version as well. An extensive discussion of the STLS approach and the results obtained within this approach was given in Ref. 5.

For the three-dimensional electron gas an analytical expression for the LFC was proposed in Ref. 30: $G(q)=A[1-\exp(-Bq^2/k_F^2)]$, with A and B as density-dependent parameters. However, in Ref. 30 the (somewhat modified) STLS equations have been solved and the *numerical* results have been *fitted* with this analytical expression. We use an analytical expression in order to solve the STLS equations in the limit of small wave numbers and in the limit of small wavelength.

Why does the analytical new SSF describe so well the transition between exchange effects for small r_s to exchange correlation effects for large r_s? The integral in the STLS approach for the LFC is essentially a q integral between 0 and $2k_F$. For small r_s we argue that $k_F\rightarrow\infty$, and the SSF is determined by $S_0(q)$; collective effects are unimportant and the important contribution to the integral comes from large q. For large r_s, on the other hand, we find that $k_F\rightarrow 0$ and the SSF is determined by the collective effects via $S_p(q)$: exchange effects are as important as correlation effects. This can be concluded from the q dependence of the SSF in the MSA.

Our results for the plasmon dispersion of the two-dimensional electron gas are in qualitative agreement with a recent theory for the repulsion hole[20] which uses the exact $G(q)$ from Monte Carlo calculations as input function. We repeat that for $1<r_s<20$ the ground-state energy calculated within the sum-rule version is in astonishingly good agreement with quasiexact Monte Carlo computations. The good agreement found for the correlation energy for $0.001<r_s<1$ indicates that the ground-state energy of interacting systems can be calculated within the sum-rule version of the STLS approach. The sum-rule version makes this task simple enough to do this calculation with a personal computer.

Essential for the CDW instability in the layered electron gas is the behavior of the LFC for small wave numbers. The LFC for small wave numbers is determined by $C_{12}(r_s)$. The behavior of $C_{12}(r_s)$ was tested by comparing the LFC and the correlation energy in the sum-rule version of the STLS approach with the results obtained by Monte Carlo calculations, and good agreement was found for $r_s<20$.

It is true that not all aspects of the LFC in the STLS approach for large r_s are reliable from a quantitative point of view. The peak in $G(q)$ near $q\sim 2k_F$ found in the numerical work for three[7] and two dimensions[18] is not found in the sum-rule version of the STLS approach. On the other hand, we believe that it is a very transparent feature of the STLS approach that for $q\rightarrow\infty$ the LFC approaches $G(q\rightarrow\infty)=\frac{1}{2}$ within the HFA. For $r_s\gg 1$ the correlation effects lead to $G(q\rightarrow\infty)=1$. The enhancement for $G(q\rightarrow 0)$ $[C_{12}(r_s)<C_{12,\mathrm{HF}}(r_s)]$ due to correlation effects is a very transparent result.

A Wigner transition to an electron crystal cannot be described by the STLS approach. The Wigner crystal is expected to occur for $r_s\sim 100$ in three dimensions,[6] and for $r_s\sim 40$ (Ref. 8) in two dimensions. Therefore, our results for the LFC for very large r_s are physically not relevant. Nevertheless, a systematic study of the pair-correlation function for small $r_s<0.5$ and large $r_s>20$ within the STLS approach has never been published. Moreover, finite width effects in the two-dimensional electron gas will shift the regime of the Wigner crystal to larger r_s.[31]

From our results it becomes clear that the STLS approach is a powerful method for studying *correlations* in interacting systems. The *exchange* contribution to many-body effects is given in terms of a simple integration over the SSF of the noninteracting system.[12] We believe that the sum-rule approach will serve as a numerical tool to study many-body effects in interacting systems with more complex interaction potentials than studied in this paper. We mention the recent study of a repulsive hard-core potential for two-dimensional electrons within the STLS approach.[32]

XI. EXPERIMENTS

In this paper we compared our results obtained within the sum-rule version of the STLS approach extensively with numerical Monte Carlo results in order to show in which density regime our approach gives quantitatively correct results. In the following we discuss some recently published experimental results where many-body effects are important or where many-body effects could be studied. For a recent review on correlation effects in solids, see Ref. 33.

A. Compressibility

In a very recent experiment[34] the compressibility of a quantum well with $L=2a^*$ has been measured, and negative values for $r_s > r_s^* = 1.7$ have been found. We believe that the experiment is qualitatively correct; however, the small-r_s^* value, where the compressibility becomes negative, is not in agreement with our theory. Actually, in the density range of the experiment the HFA can be applied, and then it is quite clear that finite width effects must increase the r_s^* compared to $r_s^* = 2.22$ for an ideally two-dimensional electron gas.[8] Therefore, we believe that the value $r_s^* = 1.7$ found in Ref. 34 is too small.

We suppose that the small-r_s limit of the measured compressibility was fixed with the results for the ideally two-dimensional electron gas. From our Fig. 6 one clearly sees that this is a wrong procedure and that the inverse compressibility of a quantum well is larger than for an ideal system. This can be discussed within the HFA: for $r_s < 10$ the exchange energy of a quantum well is strongly different from the exchange energy of the ideally two-dimensional electron gas for large density (see Fig. 9 and Ref. 4). Nevertheless, the experiment[34] is very interesting because it allows, at least in principle, an experimental determination of many-body effects.

B. Plasmon dispersion

Far-infrared measurements have already been used to study exchange effects in the two-dimensional electron gas in heterostructures as realized with $Al_xGa_{1-x}As/GaAs$.[35] However, in this experiment the density was large ($r_s \sim 0.7$) and the many-body effects were small. The q^2 quantum correction of two-dimensional magnetoplasmons, similar to the q^2 correction given in (47), has been studied in Ref. 36, though only in the $r_s < 1$ regime.

With Raman experiments the plasmon dispersion in doped semiconductors can be measured, (see Refs. 37 and 38). In GaAs with $a^* = 100$ Å the accessible q range for Raman measurements is $0.05 < qa^* < 0.3$.[35–39] The dispersion of the coupled plasmon–LO-phonon modes in n-GaAs with $N_3 \sim 8\times 10^{17}$ cm^{-3} ($r_s \sim 0.7$) was studied in light-scattering experiments.[40] We suggest studying many-body effects in semiconductors with light-scattering experiments for $r_s > 1$.

For GaAs the predicted values for $q_2 a^*$ (see Table VII and Fig. 11) are in the accessible range for Raman experiments. We find that q_2 disappears already for $r_s < 5$, in agreement with Ref. 3. Therefore, we conclude that the electron density must be small in order to observe the roton structure. However, for a small electron density the Fermi energy is small, and in order to study a degenerate electron gas in a semiconductor the measurements must be performed at low temperature $T \ll T_F$. Moreover, disorder effects might be large at low densities.

Plasmons in metals have been explored with electron-energy-loss spectroscopy.[41] Recent experiments studied the plasmon dispersion in such simple metals as Al (Ref. 42) and Na, K, Rb, and Cs.[43] For small wave numbers we express (47) as

$$\omega_p(q)/\omega_{p0} = 1 + \beta(r_s) q^2 a^{*2} + O(q^4) . \tag{64}$$

$\beta(r_s)$ versus r_s is shown in Fig. 18 together with experimental results from Refs. 42 and 43. We mention that for $r_s > 3$ the validity range of the q^2 law becomes small (see Fig. 11). It is surprising that Cs ($r_s = 5.62$) showed a weak roton structure with $\omega_p(q_2)/\omega_{p0} \sim 0.97$ and $q_2/k_F \sim 0.77$.[43] In Rb ($r_s = 5.20$) a roton structure has *not* been observed. From these experimental results we conclude that rotons appear for $r_s > 5.5$. This is in agreement with our results (see Fig. 18 and Table VII). Given the simple mode (jellium model) we use, where band-structure effects and core polarization effects[44,45] are neglected, we find this qualitative agreement with the prediction[3] of a roton structure for $r_s > 5$ very astonishing. We mention that the experiments[42,43] have been analyzed theoretically in Ref. 46 on the basis of exchange and correlation.

XII. CONCLUSION

The local-field corrections for the three- and two-dimensional electron gases have been calculated within a sum-rule version[9] of the STLS approach. An analytical expression for the static structure factor was used, where the transition between exchange effects for small r_s and exchange-correlation effects for large r_s is taken into account. We derived analytical formulas for the LFC in three dimensions and for the LFC in two dimensions,

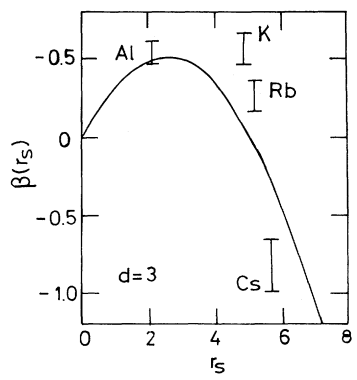

FIG. 18. Solid line: $\beta(r_s)$ vs RPA parameter r_s for three dimensions according to (64). The bars represent experimental results from Refs. 42 and 43.

which can be used as input in more complex calculations and which define the dielectric function including the local-field correction. The correlation energy calculated within this approach is in good agreement with results calculated within the Monte Carlo approach for $1 < r_s < 20$.

For the two-dimensional electron gas a roton structure in the plasmon dispersion for $r_s < 45$ has been found. A charge-density-wave instability in a layered system of electrons has been discussed. We found that correlation effects increase the instability region of a layered electron gas. Finite width effects in the two-dimensional electron gas reduce the exchange and correlation effects. We have calculated the finite width effect for the compressibility of a two-dimensional electron gas; see also Ref. 47.

For $r_s < 1$ we found good agreement between our results for the correlation energy with analytical results, and we claim that the sum-rule version of the STLS approach can also be used to study the parameter range $r_s < 1$. Finally, we mention the numerical simplicity of the sum-rule approach: the density range $0.001 < r_s < 100$ of the STLS approach has been studied within the sum-rule version. For large r_s the one-sum-rule approach might be more appropriate for certain applications of our theory. Our results for quantum wells and heterostructures indicate that the sum-rule approach can be used to obtain the corresponding numbers for exchange effects and correlation effects of structures as used in real experiments.

ACKNOWLEDGMENTS

The "Laboratoire de Physique des Solides (URA 74)" is a "Laboratoire associé au Centre National de la Recherche Scientifique (CNRS)".

[1]D. Pines and P. Nozières, *The Theory of Quantum Liquids* (Benjamin, New York, 1966), Vol. I.
[2]G. G. Mahan, *Many-Particle Physics* (Plenum, New York, 1990).
[3]K. S. Singwi, M. P. Tosi, R. H. Land, and A. Sjölander, Phys. Rev. **176**, 589 (1968).
[4]M. Jonson, J. Phys. C **9**, 3055 (1976).
[5]K. S. Singwi and M. P. Tosi, in *Solid State Physics,* edited by F. Seitz, H. Ehrenreich, and D. Turnbull (Academic, New York, 1981), Vol. 36, p. 177.
[6]D. M. Ceperly and B. J. Alder, Phys. Rev. Lett. **45**, 566 (1980).
[7]G. Senatore and G. Pastore, Phys. Rev. Lett. **64**, 303 (1990).
[8]B. Tanatar and D. M. Ceperley, Phys. Rev. B **39**, 5005 (1989).
[9]A. Gold, Z. Phys. B **89**, 1 (1992).
[10]In Ref. 8 the electron density N is missing in the expression for the SSF in the MSA.
[11]Á. A. Caparica and O. Hipólito, Phys. Rev. A **26**, 2832 (1982).
[12]J. Hubbard, Proc. R. Soc. London, Ser. A **243**, 336 (1957).
[13]J. P. Perdew and Y. Wang, Phys. Rev. B **45**, 13 244 (1992).
[14]A. Gold and L. Calmels (unpublished). Analytical results can be found in Ref. 8 for two dimensions and in Ref. 13 for three dimensions.
[15]S. Ichimaru, Rev. Mod. Phys. **54**, 1017 (1982).
[16]T. Ando, A. B. Fowler, and F. Stern, Rev. Mod. Phys. **54**, 437 (1982).
[17]F. Stern, Phys. Rev. Lett. **30**, 278 (1973).
[18]S. Moroni, D. M. Ceperley, and G. Senatore, Phys. Rev. Lett. **69**, 1837 (1992).
[19]A. Gold, Phys. Rev. B **35**, 723 (1987).
[20]D. Neilson, L. Swierkowski, A. Sjölander, and J. Szymanski, Phys. Rev. B **44**, 6291 (1991).
[21]L. Swierkowski, D. Neilson, and J. Szymanski, Phys. Rev. Lett. **67**, 240 (1991).
[22]A. Gold, Z. Phys. B **86**, 193 (1992).
[23]G. Chabrier, N. W. Ashcroft, and H. E. DeWitt, Nature **360**, 48 (1992).
[24]M. Gell-Mann and K. Brueckner, Phys. Rev. **106**, 364 (1957).
[25]A. K. Rajagopal and J. C. Kimball, Phys. Rev. B **15**, 2819 (1977).
[26]D. L. Freeman, J. Phys. C **16**, 711 (1983).
[27]S. Nagano, K. S. Singwi, and S. Ohnishi, Phys. Rev. B **29**, 1209 (1984).
[28]A. Isihara and T. Toyoda, Ann. Phys. (N.Y.) **106**, 394 (1977); **114**, 497(E) (1978).
[29]A. Isihara, in *Solid State Physics,* edited by F. Seitz, H. Ehrenreich, and D. Turnbull (Academic, New York, 1989), Vol. 42, p. 271.
[30]P. Vashista and K. S. Singwi, Phys. Rev. B **6**, 875 (1972).
[31]N. M. Fujiki and D. J. W. Geldart, Phys. Rev. B **46**, 9634 (1992).
[32]H. V. Da Silveira, M. H. Degani, and K. S. Singwi, Phys. Rev. B **46**, 2995 (1992).
[33]F. Fulde, *Electronic Correlations in Atoms, Molecules and Solids* (Springer-Verlag, Heidelberg, 1991).
[34]J. P. Eisenstein, L. N. Pfeiffer, and K. W. West, Phys. Rev. Lett. **68**, 674 (1992); J. P. Eisenstein, Superlatt. Microstruct. **12**, 107 (1992).
[35]E. Batke, D. Heitmann, and C. W. Tu, Phys. Rev. B **34**, 6951 (1986).
[36]E. Batke, D. Heitmann, J. P. Kotthaus, and K. Ploog, Phys. Rev. Lett. **54**, 2367 (1985).
[37]T. Egeler, G. Abstreiter, G. Weimann, T. Demel, D. Heitmann, P. Grambow, and W. Schlapp, Phys. Rev. Lett. **65**, 1804 (1990).
[38]A. R. Goñi, A. Pinczuk, J. S. Weiner, J. M. Calleja, B. S. Dennis, L. N. Pfeiffer, and K. W. West, Phys. Rev. Lett. **67**, 3298 (1991).
[39]T. Egeler, S. Beeck, G. Abstreiter, G. Weimann, and W. Schlapp, Superlatt. Microstruct. **5**, 123 (1989).
[40]G. Abstreiter, R. Trommer, M. Cardona, and A. Pinczuk, Solid State Commun. **30**, 703 (1979).
[41]H. Raether, *Excitations of Plasmons and Interband Transition by Electrons,* Springer Tracts in Modern Physics Vol. 88 (Springer, Berlin, 1980).
[42]J. Sprösser-Prou, A. vom Felde, and J. Fink, Phys. Rev. B **40**, 5799 (1989).
[43]A. vom Felde, J. Sprösser-Prou, and J. Fink, Phys. Rev. B **40**, 10 181 (1989).
[44]K. Sturm, Solid State Commun. **27**, 645 (1978).
[45]M. Taut, Solid State Commun. **65**, 905 (1988).
[46]Ll. Serra, F. Garcias, M. Barranco, M. Barberán, and J. Navarro, Phys. Rev. B **44**, 1492 (1991).
[47]A. Gold and L. Calmels, Solid State Commun. (to be published).